BUCKLING AND STRENGTH ANALYSIS OF PANELS WITH DISCRETE STIFFNESS TAILORING

Lucie Culliford[1], Rizwan Saeed Choudhry[2], Richard Butler[1] & Andrew Rhead[1*]

[1] Materials and Structures Research Centre, Department of Mechanical Engineering, University of Bath, Bath, UK
[2] Department of Mechanical Engineering and Built Environment, College of Engineering, University of Derby, Derby, UK
[*]corresponding author

ABSTRACT

Continuous variation of stiffness across flat plates has been shown, theoretically, to improve buckling performance by up to 60%. However, steered fibre manufacturing methods cannot achieve the minimum radius of curvature required for improvement whilst maintaining a high deposition rate. An alternative concept, Discrete Stiffness Tailoring (DST), which varies stiffness within a ply through discrete changes of angle, is compatible with high rate deposition methods such as Advanced Tape Laying. Through the simple example of redistribution of the material in a quasi-isotropic $[\pm 45/90/0]_{2S}$ laminate whilst maintaining ply percentages, DST is shown both experimentally and theoretically to improve buckling stress by at least 15% with no indication of failure in regions of discrete angle change (seams). However, the reduced tensile strength of seams obtained by virtual and experimental testing means that increased buckling performance in the principle load direction needs to be balanced against loss of transverse strength.

1 INTRODUCTION

Ever present demand for fuel efficiency in the aerospace industry is driving efforts to realize the full potential of composite materials in terms of weight reduction and performance optimization. Previous work has shown that one aspect of this effort, buckling performance, can be improved by stiffness tailoring. Theoretical parametric work conducted by Biggers et al. identified that the redistribution of very stiff (e.g. 0^o plies) to the outer regions of a compressive panel would produce an increase in the buckling load [1] for uni-axial compression. However, subsequent work on buckling optimization of panels via spatial variation of stiffness has predominantly focused on using continuous curvilinear fibre steering [2-5]. A review of variable stiffness laminate designs for buckling [6] reports that the achievable buckling load capacity of a tow steered flat plate may be limited by the manufacturable steering radius of the fibres. For example, Dodwell et al. [7] have shown that if angle and ply thickness are simultaneously varied across the width of a compression panel, a weight saving of up to 40% can be achieved provided that the fibre steering radius can be precisely controlled (<30mm). Continuous Tow Shearing (CTS) [8] is a method of fibre steering that can achieve such control, however it is not currently suited to high rate manufacture. Discrete Stiffness Tailoring (DST) is based on the idea of Automated Tape Laying (ATL) of bi-angle Non-Crimp Fabrics (NCFs) and has potential to offer significant manufacturing benefit. The one-dimensional ATL method [9] adopted by DST laminates can, theoretically, lay down material up to 4 times faster than a standard unidirectional lay-up where, for instance, ±45° plies require a change in the tape head laying orientation. Combining this method with the use of bi-angle NCFs can result in deposition rates eight times greater than currently achieved [9]. Such an approach circumvents quality issues resulting from requirements for low fibre steering radii in continuous steering methods. Furthermore, results in [7] theoretically demonstrated that equal weight savings to steered fibre CTS panels may be achieved with as few as three discrete strips of straight fibres, each with a different fibre orientation. This is because in a DST laminate, ply thickness and angle are altered discretely and independently across the geometry of a structure. Optimised DST designs are theoretically able to achieve a 40% weight saving compared to an optimized straight fibre design with equal buckling performance [7].

However, although both continuous and discrete fibre steering have been shown to improve buckling resistance, they also create regions of high stress that are susceptible to growth of damage. In a DST laminate, the point at which one orientation terminates and another commences (a seam) creates vulnerability in the structure. In this paper, the concept of DST is used to redistribute material within a standard ply quasi-isotropic (QI) laminate without loss of in-plane stiffness. Improvements in buckling performance are assessed using numerical and experimental methods. Two different ways of staggering seams are explored and experimental and numerical tensile testing is used to evaluate their impact on transverse tensile strength.

2 PANEL DESIGN AND MANUFACTURE

DST uses discrete angle variation to enable component manufacture where stiffness is tailored in different zones to enhance the buckling performance of the structure, see Fig. 1. Gürdal et al. [2] studied two cases of tow paths which linearly vary along the longitudinal x direction or the transverse y direction. Results indicated that, due to redistribution of the longitudinal compressive load N_x, fibre angle variation in the y direction is more efficient than variation in the x direction in the case of initial buckling.

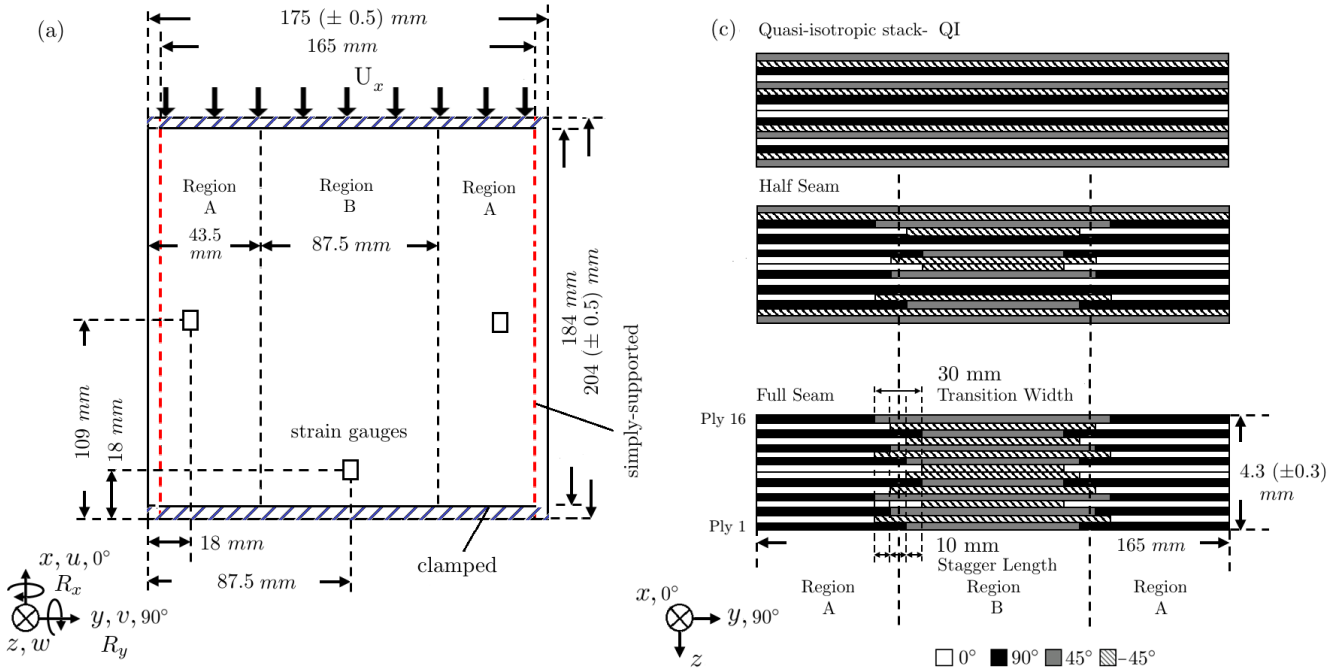

(d)

Panel Name	Region A	Region B
QI	$[\pm 45/90/0]_{2S}$	$[\pm 45/90/0]_{2S}$
Half Seam	$[\pm 45/(90/0)_3]_S$	$[\pm 45_2/(90/0)/\pm 45]_S$
Full Seam	$[\pm 45]_{4S}$	$[90/0]_{4S}$

Figure 1: (a) Plan view of a DST compression coupon showing idealised boundary conditions, panel dimensions and loading regime for buckling tests. Red dashed lines indicate simply-supported boundary conditions. (b) Plan view of DST tensile coupon. (c). Not-to-scale cross-sectional representations of the QI, Half Seam and Full Seam stacking sequences showing staggered seams. (d) Table of stacking sequences for each panel and both regions.

Therefore, in this paper, in order to achieve the best structural efficiency whilst retaining prismatic conditions required for VICONOPT analysis (see Section 3), stiffness variation is only considered in the direction transverse to load. Stacking sequences and panel design are based on the simple premise of redistributing 0°, ±45° and 90° material (without altering the relative volume or angle of 0°, ±45° and 90° material and based on stiffness redistribution concepts highlighted in [10]) in a balanced symmetric quasi-isotropic laminate to bring about buckling performance improvements, see Fig. 1. Such a design experiment offers a simple way to demonstrate the potential for DST buckling improvements, whilst offering a simple example against which analysis methods can be tested. However, it is worth noting that these designs *are not* optimized for performance; theoretical optimal designs for flat plates can be found in [5].

Two methods for DST were considered; 'Full seam', where all plies have discrete junctions between material with different fibre angles and 'Half seam' where 50% of plies contain junctions or 'seams'. Each concept offers different degrees of continuity to the seams, see Fig. 1. Panels were manufactured, as per the stacking sequences and seam regions given in Fig. 1, using HTS40/977-2 material with material properties summarized in Table 1. Regions A and B in Fig. 1 are partitioned by transitional regions in which discrete changes in ply orientation occur. Ply orientations are altered over a 30mm wide region, with neighbouring seams being staggered by 10mm.

As the seam region is expected to reduce the transverse strength of the panels [10], three types of tensile coupons based on the buckling coupon designs were created, see Fig. 1(b) and (d). Note that the seamed tensile specimens isolate a single seam straddled by Regions A and B, see Fig. 1(b).

3 NUMERICAL ANALYSES FOR BUCKLING AND STRENGTH

In order to design and optimise DST panels efficiently in future, it must be proven that computationally efficient methods for assessing buckling performance and seam strength can be utilised or adapted for use with DST panels. As such, the methods for analysing buckling performance outlined below have deliberately been constrained to those that are in standard use and are computationally efficient. The predictive capabilities of these models and thus their use in future design studies will form part of the discussion of this paper.

3.1 Methods used to assess buckling performance

Two methods are employed for determining buckling performance of the QI, Half seam and Full seam panels; Finite Elements and the finite strip program VICONOPT [11].

3.1.1 VICONOPT buckling analysis method

Most aerospace structures, such as wing and fuselage panels, are long compared with cross-sectional dimensions. Hence, Strip models, that make prismatic assumptions, are computationally efficient in many applications although approaches that find buckling loads by minimizing potential energy for assumed mode shapes have also been developed [12]. VICONOPT, a computationally efficient method suitable for implementation with parallel computing methods, has previously been used to predict buckling performance of DST laminates [7]. It was shown that the distribution of alternative ply orientations within a flat panel has greater impact on delaying the onset of buckling than altering the thickness along the width [7] and so experiments in this paper are constrained to angle variation only. For panels and loadings that are prismatic in the x direction and under the assumption that there is no coupling between in-plane and out-of-plane deformation (i.e. the $\boldsymbol{B}$ matrix of classical lamination theory is null), VICONOPT provides infinite periodic solutions to the equilibrium equation that governs buckling;

$$D_{11}\frac{\partial^4 w}{\partial x^4}+4D_{23}\frac{\partial^4 w}{\partial x\partial y^3}+2\left(D_{12}+2D_{33}\right)\frac{\partial^4 w}{\partial x^2\partial y^2}+4D_{13}\frac{\partial^4 w}{\partial x^3\partial y}+D_{22}\frac{\partial^4 w}{\partial y^4}+\left(N_x\frac{\partial^2 w}{\partial x^2}+2N_{xy}\frac{\partial^2 w}{\partial x\partial y}+N_y\frac{\partial^2 w}{\partial y^2}\right)=0 \tag{1}$$

Where N_x , N_y and N_{xy} are in-plane forces and D_{11}, D_{12}, D_{22}, D_{13} and D_{33} are the bending stiffness terms of classical lamination theory. Solution of Eq. (1) is via exact, periodic formulations [13] of the form:

$$w = f_1(y)\cos\frac{\pi x}{\lambda} - f_2(y)\sin\frac{\pi x}{\lambda} \tag{2}$$

where the functions $f_1(y)$ and $f_2(y)$ allow various boundary conditions to be applied on the longitudinal edges of panels, including free, simple, clamped and elastic supports. The half-wavelengths λ in Eq. (2) are defined by the length of the plate L divided by the number of half-wavelengths assumed along the length of the plate. VICONOPT divides the panel under investigation into strips across its width. In a DST panel each strip will have a different set of bending stiffnesses and, in the results that follow, 13 to 18 strips are used depending on the presence of transition regions. Buckling load factors are derived through an eigenvalue analysis which is executed on the transcendental stiffness matrix derived from the solution of the governing differential equations of the constituent strips. The transcendental eigenproblem requires an iterative solution that is performed using the Wittrick-Williams algorithm [14]. The lowest buckling load found for a range of values of λ is taken as the critical buckling mode for the panel.

3.1.2 Finite Element buckling analysis method

Finite element buckling and strength analysis was carried out using commercially available software package ABAQUS™ Standard [15] in order to (i) confirm the predictive capacity of VICONOPT simulations, (ii) investigate alternative boundary conditions, (iii) explore non-linear buckling behaviour of the panels, and (iv) model the strength of the seams. Eigenvalue buckling analysis (perturbation method) [16] was used to estimate

buckling stress and strain. Non-linear FEA continuation analysis [16] was used, for capturing the post-buckling path. Since the QI panel has a trivial fundamental path, an imperfection in the form of bifurcation mode having the lowest bifurcation load was applied to the mesh. An imperfection magnitude of $\delta_o = t_h/100$, where t_h is the thickness of the laminate, was used. Solutions used the Riks (Arc length) [17] method based solver in ABAQUS. In the case of the Half seam and Full seam panels, due to the material asymmetry in the transition zone, it is not necessary to force an artificial imperfection. Thus, for these cases it was sufficient to use the geometrically non-linear solver (employing a Newton method) in ABAQUS [15] with incrementally increasing loads to capture the bifurcation point and post-buckling path.

Each panel was modelled with a mesh consisting of 30360 S8R doubly curved thick shell elements each having 8-nodes, quadratic reduced integration and an edge length of around 1mm. A mesh convergence study was carried out. The complete panel was modelled as a single part with uniform mesh density. A lamina type [15] material definition was used for each layer and the orthotropic material constants for the unidirectional HTS40/977-2 CFRP material are summarized in Table 1 [18, 19]. The layup sequence corresponding to each part for each region (as described in Fig 1(d)) was specified as part of the section definition in ABAQUS using the composite layup tool and by creating appropriate partitions for each zone.

3.2 Finite Element method for tensile strength

In this study, finite element analysis of DST panels under tension was undertaken with a view to understanding the failure process. This was accomplished by studying the evolving stress state, resulting from the progressive damage growth from the seams that connect regions of dissimilar stiffness. Finite element simulations were carried out using ABAQUS™/Standard. Geometrically non-linear (large displacement) analysis was carried out for modelling damage growth. Cohesive zone modelling (CZM) [20] was used to simulate both the inter-laminar and intra-ply crack growth at the seams. Other ply damage mechanisms were not modelled directly; rather the failure indices for these modes were evaluated during post processing at various load steps to understand the evolving nature of damage within the test panels. The model assumed a plane strain (in the *y-z* plane) representation of the tensile panel in Fig. 1(b), thereby ignoring free edge effects. Each ply, its associated polymeric inter-laminar interface region as well as polymeric seams that define the transition between sections of different fibre orientation were modelled discretely and separate material models were defined for each zone. The material behaviour for each ply was assumed to be linear-orthotropic. Although previous studies by Atas et al. [19] suggest that ±45 plies in tension can display highly nonlinear shear behaviour it was decided not to include this description into the material model for the tensile simulations. Instead, the intention here is to establish an indication of stress levels and damage in the seams; accounting for non-linear shear of plies (whilst not accounting for ply failure as noted above) would only complicate the model, with little change in accuracy in the seamed region.

In order to simplify the modelling of seam failure, it was assumed that crack propagation would take place purely within the inter-ply resin region (polymeric seam) as opposed to being an interface crack (de-cohesion failure). Hence, seams were modelled as a solid layer with embedded cohesive zone (red elements in Fig. 2) along the mid-plane of the seam. An isotropic material definition based on the material properties of Epoxy-977-2 was used for the solid region while the embedded cohesive zone was defined using a traction-separation law and mixed-mode failure governed through the BK-criteria [21]. Material properties for all regions are given in Table 1. Figure 2 illustrates the converged finite element mesh where the following element dimensions were used for each of the zones: plies 62.5 μm x 50 μm, inter-laminar regions 4 μm x 5 μm and intra-ply seams 18 μm x 2.5 μm. As shown, a refined mesh (1.629 million and 1.630 million elements for the Half and Full seam cases respectively) was used to capture stress gradients between zones of different stiffness accurately and to enable stable propagation of damage within the cohesive zones. Following Dizy et al. and the ABAQUS Manual [22, 23], regions in Fig. 2 were connected using node-based tie-constraints applied at mating surfaces (edges). Tie-constraints were used to connect the non-matching meshes of the ply regions (fewer elements) and the interface and seam regions (more elements) allowing overall for a computationally tractable model with higher fidelity in the interface and seam regions. It was possible to use fewer elements in the ply region as the resolution of the stress field here would see minimal benefit from a high fidelity mesh especially as the use of solid elements to connect ply and interface regions allowed for a smooth transition of strain field between the two zones. All simulations were convergent beyond the maximum loads observed in the experiments but eventually became non-convergent at higher loads following numerical instabilities relating to fast fracture in inter-laminar seam regions.

4 EXPERIMENTAL METHOD

Compression and tensile testing were carried out to assess buckling capacity and tensile strength as described in Fig. 1. Tensile tests were designed to assess the transverse load carrying capability of the compression panels. Hence, the relative orientation of fibre directions and loads in Figs. 1(a) and (b) should be noted.

4.1 Compression test method for buckling performance of DST panels

Fifteen buckling panels were manufactured with dimensions in Fig. 1(a), five QI with no seams and five of each seam type. Panels were compression tested using an Instron 5585H machine, at a displacement rate of 0.1 mm/min applied in the 0° direction of the coupons. Specimens were supported in a modified version (increased gauge width and height) of the test fixture described by ASTM D7137 [24] with the exception that loading edges were clamped to prevent 'brooming' type end failures, see Fig. 1. All coupons were monitored with 6 strain gauges with positions given on Fig. 1. A Spider 8 data acquisition system and Catman software [25] were used to capture strain and load data. A Limess Digital Image Correlation (DIC) system employing a stereo pair of 1MP high speed Photron SA3 Cameras was used to track coupon strain and displacement in three dimensions. Post-processing was undertaken using Correlated Solutions' VIC3D software [26].

Orthotropic Elastic Properties of UD HTS 40/977-2					
E_{11T} (GPa)	E_{11C} (GPa)	E_{22} (GPa)	ν_{12}	$G_{12} = G_{13}$ (GPa)	G_{23} (GPa)
135.405	112	10.3	0.3	5.2	3.43
Orthotropic Strength Properties of UD HTS 40/977-2					
X_T (MPa)	X_C (MPa)	$Y_T = Z_T$ (MPa)	$Y_C = Z_C$ (MPa)	$S_{XY} = S_{XZ} = S_{YZ}$ (MPa)	
2540	1500	82	236	101	
Strength Properties of $[\pm 45]_{2S}$					
Tensile Strength (MPa)		In-Plane Shear Strength (MPa)		In-Plane Shear Yield (MPa)	
202		101		52	
Properties of Epoxy 977-2					
E (GPa)	ν	Strength (MPa)			
3.5	0.38	81			
Cohesive Zone Properties					
K_n (N/mm^3)	K_t (N/mm^3)	Normal Strength (MPa)	Shear Strength (MPa)	G_{IC} (N/mm)	G_{IIC} (N/mm)
1.00E+05	1.00E+05	60	80	0.352	1.45

Table 1: Summary of material properties [18, 19].

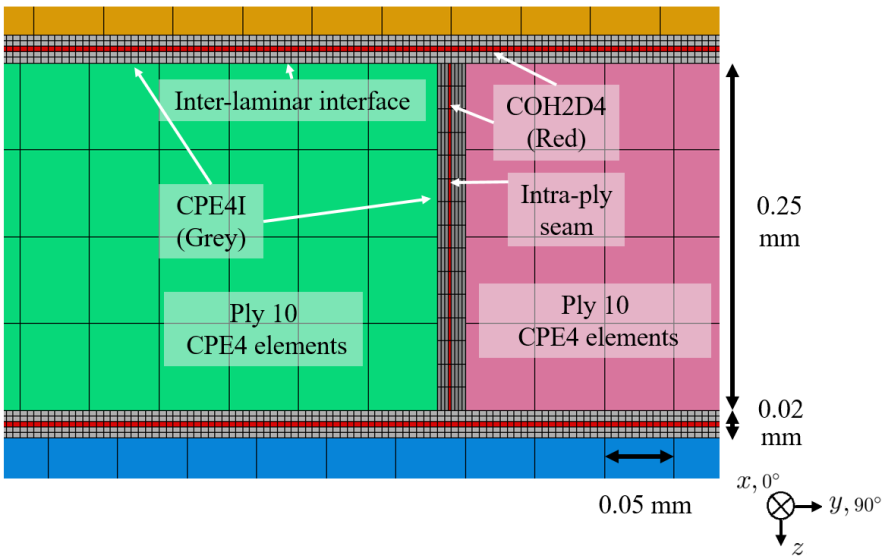

Figure 2. Illustrative FEA cross-section details for the tensile damage model indicating element types used in various regions.

4.2 Tension test method for transverse strength of DST panels

Fifteen tensile coupons were manufactured, five QI with no seams and five of each seam design. All coupons were tested under tension in an Instron 5585H uni-axial test machine with loading applied in the 90° ply direction (relative to the compression panel loading direction). Load was applied via gripping of sections of the coupons that had been tabbed with 2mm aluminium sheet as per Fig. 1(b). The initial Full and Half seam coupons were loaded at a fixed displacement rate of 0.2 mm/min, which was then increased to 0.6 mm/min in all subsequent tests. An extensometer and DIC system (as described above) were used to monitor strains and displacement.

5 RESULTS

5.1 Buckling performance

Experimental buckling results are plotted alongside VICONOPT and FEA analyses in Fig. 3. Triangular and circular markers indicate clamped and simply-supported loading edges in the numerical models respectively. With the minor exception of the lowest experimental Half seam buckling stress result, these numerical results fully bound those experimentally obtained in Fig. 3(a). The bifurcation point for each experimental test was determined by using the average strain data of all six gauges to locate the point at which a significant stiffness change was observed, see Fig. 4. At this point, the two linear regions either side of that kink were extrapolated until they crossed each other. The stress at which they met, calculated from the experimental loads and cross-sectional area for each panel, was taken as the buckling stress of the panel. At this buckling stress, the average strain for all six gauges was taken as the buckling strain result, plotted in Fig. 3(b). The experimentally recorded strains are consistently below the numerical predictions. The stiffness pre and post buckling was also determined from the average strain data, Fig. 4. Buckling stress results were confirmed by tracking the central deformation of buckling mode shapes using DIC, see Fig. 5. Comparative buckling mode shapes from experimental results for all panels are given in Fig. 6. FEA for the QI panel, under both pinned and clamped boundary conditions, are shown in Fig. 6(d). The Half and Full seam numerical FEA mode shapes are indistinct to those produced for the QI panel. VICONOPT mode shapes were also indistinguishable from FEA mode shapes.

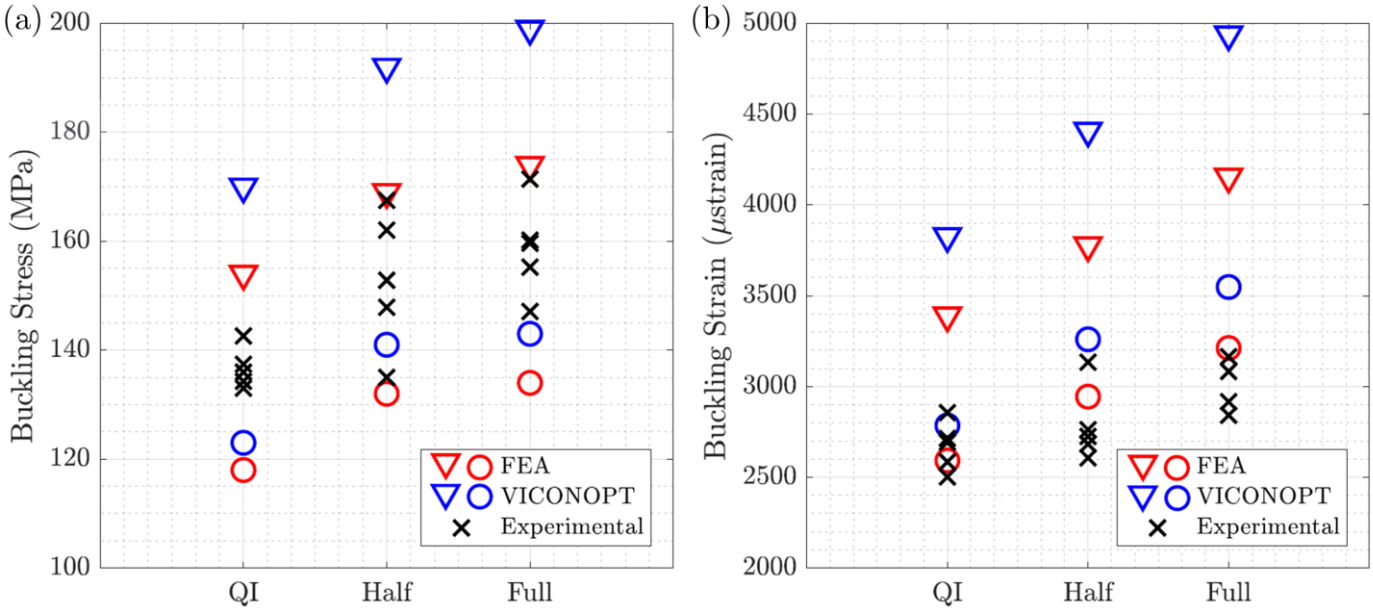

Figure 3. (a) Comparison of buckling results obtained from VICONOPT, FEA simulations and all experimental compression tests. Triangular markers denote clamped loading boundaries in the numerical simulations, circular markers relate to simply-supported loading boundaries. In both cases the non-loading edges are simply supported. VICONOPT and FEA use the width between the supports (165mm) for the calculation of stress, whereas the experimental results use the full width (175mm). (b) Buckling strain comparison, presented as in (a).

5.2 Tensile strength of seams

Figure 7 (a) and (b) presents example experimental and FEA stress versus strain curves for Half and Full seams respectively. Experimental strains are derived from DIC data from the first coupon test (No. 1) for all configurations. For each case, the seam coupons strains were extracted from both Regions A and B (25mm and 75mm along the gauge length respectively) at the mid-width of the coupons. The QI coupon stress vs. strain results were linear, with sudden failure as expected at an average stress of 691 MPa. Average experimental failure stresses for the Half and Full seam tensile tests were 369MPa and 179MPa respectively. FEA strains were extracted at corresponding locations in Ply 1 (lower most ply – see Fig. 1(c)), for both the Half seam and Full seam cases. The inset FEA diagrams in Fig. 7 describe the evolution of seam damage (both inter-laminar and intra-laminar) with increasing load (nominal stress). Only the largest seam damage zone within the specimen is shown. For both the Half and Full seam case, the three insets correspond to (i) the initiation of damage within the seam, (ii) the full degradation of the seam and the onset of damage propagation to the interlaminar region, and (iii) the maximum damage state at the end of the converged simulation.

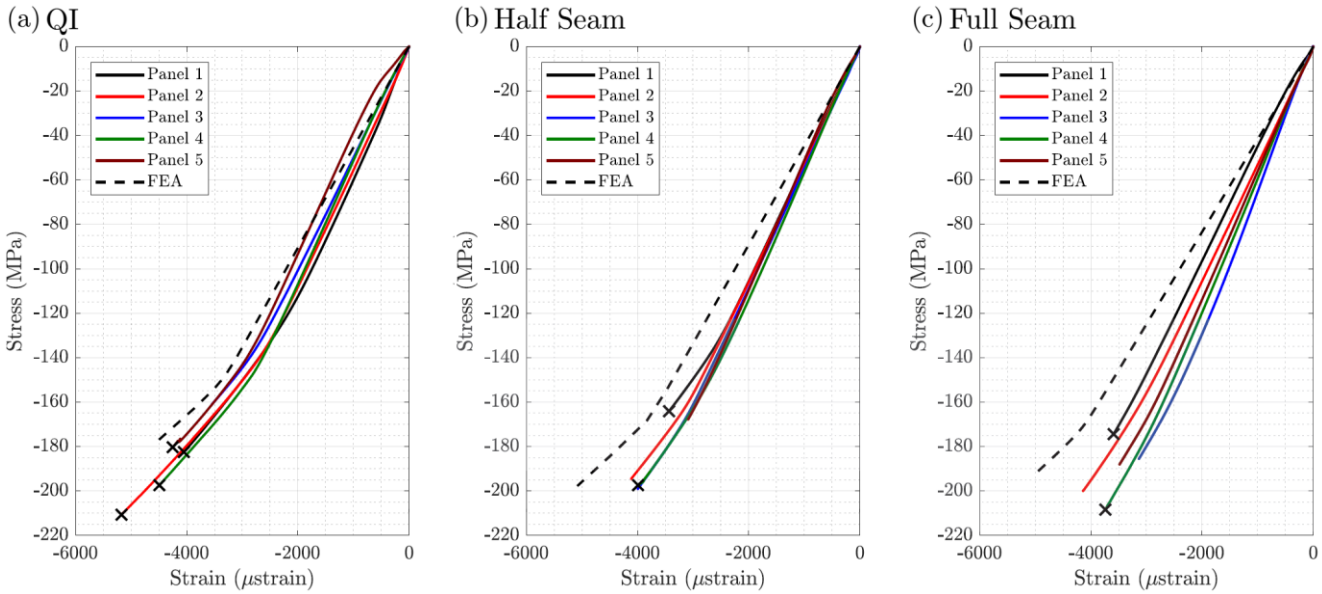

Figure 4: Stress vs. averaged strain results based on strain gauge readings for (a) QI panel, (b) Half Seam panel and (c) Full Seam panel. The average of all six strain gauges is presented. Results from the FEA simulation (loading edges are simply supported) are presented for each panel type. The crosses indicate failure of the panel for some tests.

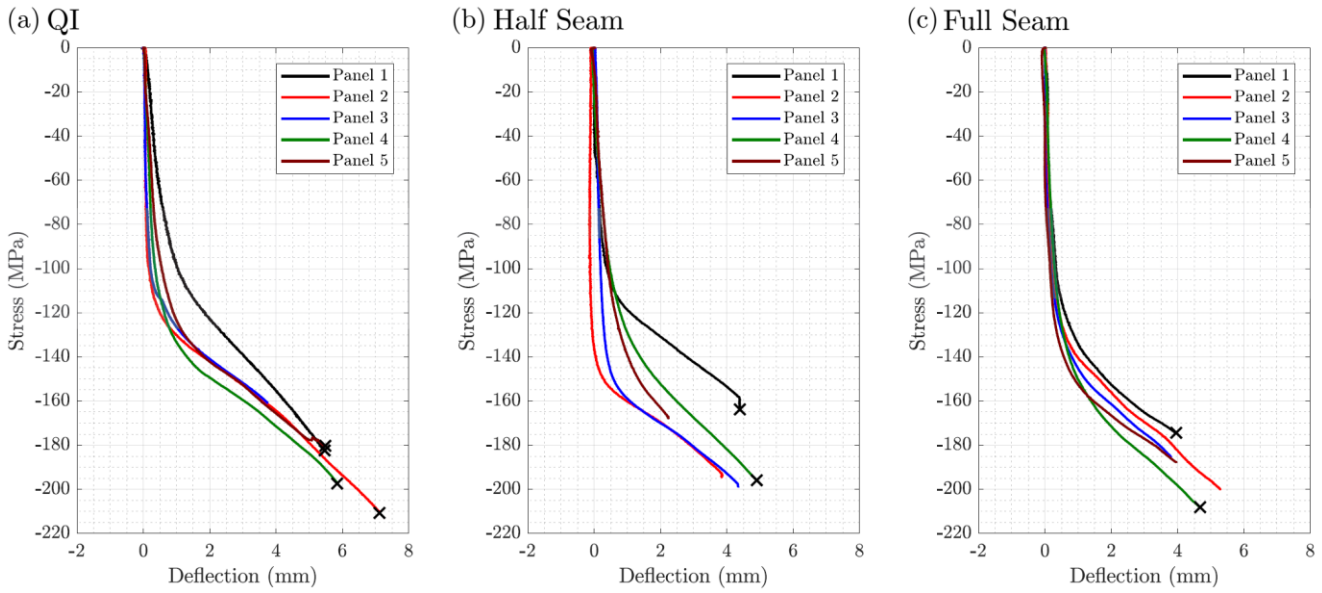

Figure 5: Stress vs. the absolute value of out-of-plane deflection, taken from the DIC analysis from the centre of the buckle.

An example of surface ply strain for key points during the tensile tests are shown in Figure 8(a) using a set of DIC images. In Figure 8(b) the through-thickness failure index (FI) for each ply has been plotted using FEA results. The failure index is based on max longitudinal stress criteria FI = σ_{yy} / S^{θ} where σ_{yy} is the longitudinal stress at each integration point within a ply and S^{θ} is the longitudinal strength of the ply at a particular orientation θ. Thus, for a ply of ±45°, S^{θ} = 202MPa, for a 90° ply, S^{θ}= 82MPa, and for a 0° ply, S^{θ}= 2540MPa (see Table 2). A value of ≥1 indicates onset of damage within the ply and <1 indicates that the ply is undamaged.

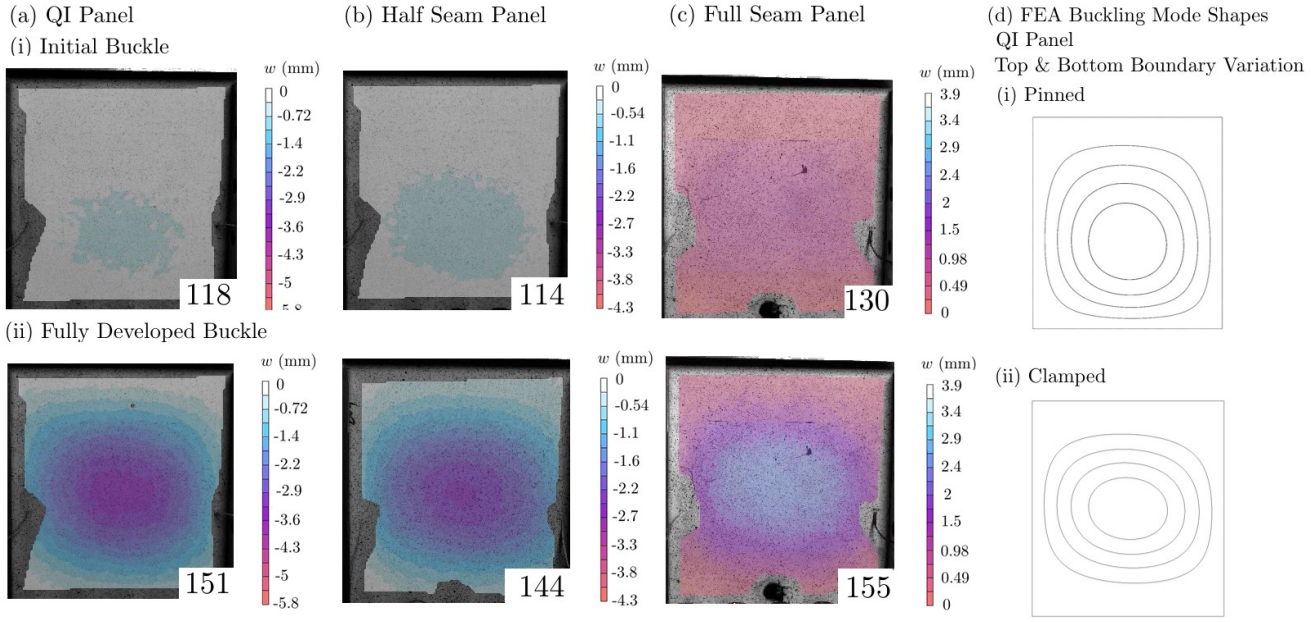

Figure 6: Example DIC images, taken from Panel 1 tests, of out-of-plane deflection indicating the emergence of buckling mode shapes (a) QI (b) Half Seam and (c) Full Seam. The stresses (in MPa) at which these images were recorded are given in the bottom right corner. The buckling mode shapes for the QI panel, obtained by FEA, with pinned and clamped boundary conditions are shown to the right of the DIC images.

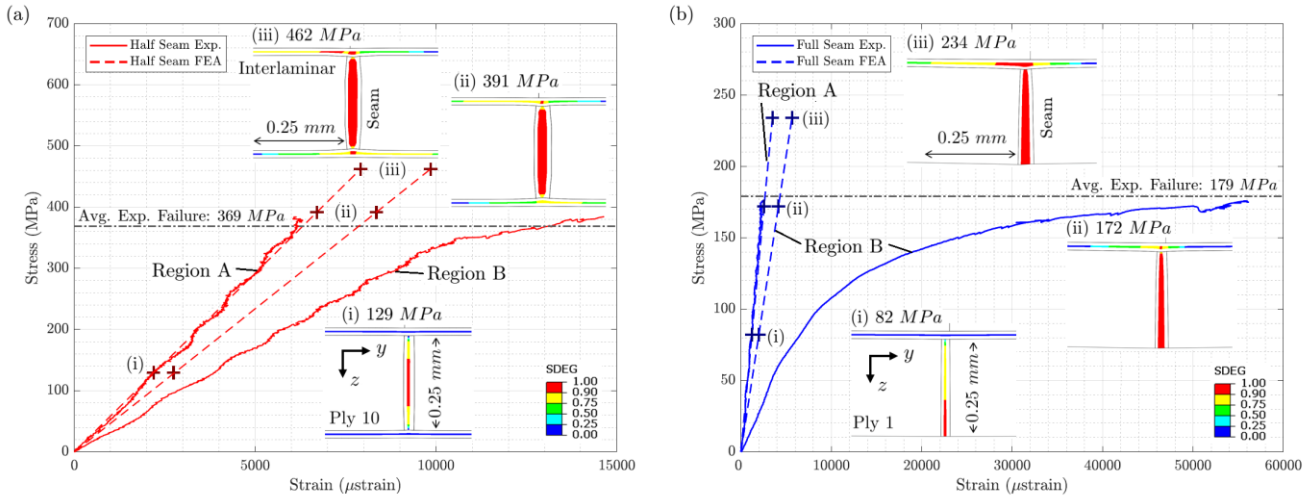

Figure 7: FEA and experimental strain vs. stress results for the tensile tests on set of coupons 1 (a) Half Seam and (b) Full Seam. Regions A and B are described in Fig. 1. The crosses denote points at which the growth of seam damage in the seam and interlaminar region was evaluated using FEA; (i) initiation of damage, (ii) full development of seam failure and damage propagation from the seam into the interlaminar region and (iii) fully developed damage in the seamed region.

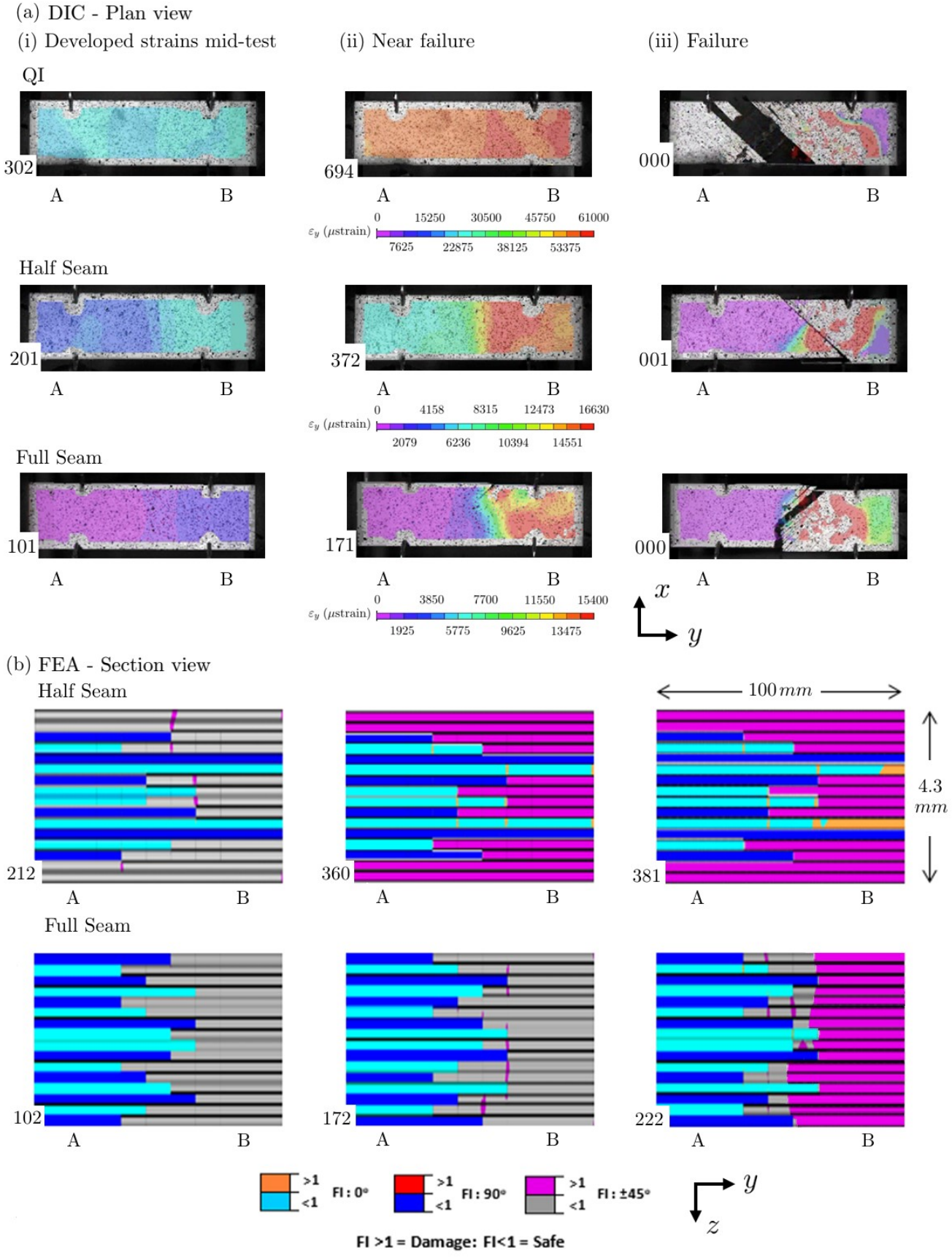

Figure 8: DIC strains and FEA ply failure progression at key levels stress for Half Seam and Full Seam coupons (a) DIC planar images of tensile strains developed during testing; note the different strains developed in different halves of the coupons. Stresses (in MPa) are given in the bottom left of each image. (b) FEA Cross-section images showing both initiation of damage, and extensive ply failure around the seam region. Stress is displayed as in (a). Regions A and B are indicated below the images.

6 DISCUSSION

6.1 Buckling performance

VICONOPT and FEA numerical results predict an increase in buckling stress of between 8.3-12.7% and 11.5-14.6% for the Half and Full seam panels with respect to the QI panel (the range being boundary condition dependent, see Fig. 3). FEA predicts lower buckling load and stress values in all cases but is within 13% of VICONOPT results. This is a consequence of different boundary conditions in the two methods: in the FEA, the longitudinal supports (parallel to the *x*-axis) induce a secondary stress in the panel due to Poisson's ratio thereby causing buckling to occur at a lower load. In VICONOPT the strain is applied within the panel and no transverse stress is assumed.

The improvement in DST buckling stress seen in theoretical results is matched by experimental buckling results which show an increase in buckling stress of 11.4% using a Half seam design, and 16.8% using a Full seam design. Considering buckling strain instead, a comparison of results in Fig. 4(b) shows no noticeable difference between the experimental QI and Half seamed panels, but the Full seam produces a 17% increase in average panel buckling strain. However, there is an inherent difficulty in determining the precise bifurcation point for each test, and normal manufacturing errors in ply orientation and seam positioning must apply. Hence, a Mann-Whitney U statistical test was used to determine whether the difference in buckling stress between the Half and Full seamed panel experimental results and those of the QI panels were statistically significant. Using $\alpha < 0.01$, (the lowest limit of acceptable level of significance (magnitude of difference) is $\alpha = 0.05$) the U-test shows that the Full seam buckling stress results are significantly different when compared to the QI baseline. Similarly, a two sided t-test for the Half and Full seamed panels provides sufficient evidence ($\alpha = 0.05$) to accept the original model hypothesis for buckling stress improvements of at least 14.6% with a simply-supported boundary condition. Hence, a comparison of analytical models and experimental buckling results shows that both ABAQUS and VICONOPT can be used to optimise DST panels and structures in future.

6.2 Tensile strength

Failure of the QI coupons was recorded at an average of 690 MPa with sudden failure in the middle of the gauge length, see Fig. 8(a). The average final failure stress of the Half and Full seam coupons were 47% and 74% lower respectively. For both seam cases, failure images in Fig. 8(a) show significant cracking in ±45° plies, with the majority of damage and considerably higher strains seen in Region B. Similarly, post-test visual inspection indicates overall failure was likely not a result of seam failure although some interaction of damage within the seam is seen for the Full seam test in Fig. 8(a). This corresponds both with Fig. 7, which shows non-linear behaviour in the ±45° ply dominated Region B, and the failure index analysis in Fig. 8(b), which shows the onset of ply failure, mainly in the ±45° plies in Region B, at loads considerably below the experimental failure load. As Fig. 7 shows that Region A has a linear stress-strain response (predicted by the FEA for both seam cases) it is apparent that the discrepancy in failure stress between QI and seamed tests is a principally a result of failure in Region B.

As the aim of the tensile FEA model was to understand seam failure, progressive damage was only considered for the seam interfaces and not within the plies themselves. This meant the non-linear stress-strain relationship, resulting from non-linear ply deformation and fracture in Region B was not captured by cohesive failure of the resin regions around seams, see Fig. 7. However, the first onset of interlaminar damage following resin failure at the end of terminated plies coincides well with ultimate failure loads, see Figs. 7(a)(ii) and 7(b)(ii). Similarly, contrasting ply failure indices in Fig. 8(b) with experimental failure loads (see Section 5) shows ply failure is broadly indicative of ultimate coupon failure; FEA stresses for the Half seam, that correspond to initiation and widespread failure of ±45° and 90° plies (perpendicular to the tensile load), bound the average experimental result for failure. Similarly, FEA stresses relating to initiation and extensive failure of ±45° plies in Region B bound the average experimental failure stress for the Full seam case.

FEA predicts that the failure of the resin regions at the end of plies within seams initiates without loss of stiffness at the coupon length scale. By noting the linearity of experimental stress vs. strain data in Fig. 7, near the stresses suggested by FEA in Fig. 8(b), it is apparent this is consistent with the experimental results for Region A. Buckling tests that ended in failure of the panel are marked in Figs. 3 and 4. However, these failures were not seam related and post-test visual analysis of the panels shows no damage to the seamed regions. Thus with the caveat that optimisation for buckling may further increase stress in seamed regions, it can be concluded that (i) for uni-axial

compressive load with seams parallel to the load, reduction in strength due to DST does not seem to be critical and (ii) uni-axial buckling loads and tensile strength of seamed coupons can be predicted by readily available numerical methods. The simple FEA model introduced in this paper could form a basis for seam design, as the stress at which the interlaminar damage initiates appears to provide a good approximation of seam strength. Additionally, Czel et al. [27] have previously noted the benefits for damage detection and load redistribution for structures containing ply discontinuities that may assist with aircraft certification.

7 CONCLUSIONS

Use of Discrete Stiffness Tailoring (DST) to affect simple redistribution of 0°, ±45° and 90° material (whilst maintaining the volume of each) has been shown, in a statistically significant manner, to improve buckling performance of Half and Full seamed panels, both experimentally and numerically, by up to 11% and 15% respectively in comparison to a $[45/-45/90/0]_{2S}$ laminate.

FEA and VICONOPT buckling analyses, that are sufficiently computationally efficient to be used in initial design studies, are shown to capture relative performance differences between control, Half and Full seam DST panels to <5%. Both methods are also found to agree with experimental values to within 10% when simply-supported boundaries conditions are applied along the loading edges.

When aligned perpendicular to compression loading, in-plane seams created by the DST process are seen to have limited or no effect on buckling performance and compression strength/modulus. Tensile testing and accompanying FEA predictions indicate that tensile strength is reduced for seamed laminates but that it can be predicted to a reasonable degree by FEA analysis.

Overall, given the size of seam regions on production aircraft structures and the likely ratio of primary and secondary loadings on aerospace components, results indicate that DST should be a suitable manufacturing process for improving laminate structural efficiency.

8 ACKNOWLEDGEMENTS

This work was supported by the ADAPT EPSRC grant number EP/N024508/1 which is gratefully acknowledged. Richard Butler is supported by Royal Academy of Engineering and GKN Aerospace Research Chair. Lucie Culliford's PhD studentship is 50% funded by GKN Aerospace.

REFERENCES

[1] S.B. Biggers & S. Srinivasan, Compression Buckling Response of Tailored Rectangular Composite Plates. *AIAA Journal,* **31**, 1993, No. 3, pp. 590-596.

[2] Z. Gurdal & R. Olmedo, In-Plane Response of Laminates with Spatially Varying Fiber Orientation: Variable Stiffness Concept. *AIAA Journal,* **31**, 1993, No. 4, pp. 751-758.

[3] M.W. Hyer & R.F. Charette, The Use of Curvilinear Fiber Format in Composite Structure Design. *AIAA,* 1989. Paper No. 1989-1404.

[4] E. Lund, Buckling Topology Optimization of Laminated Multi-Material Composite Shell Structures. *Composite Structures,* **91**, 2009, pp. 158-167.

[5] Z. Wu, P.M. Weaver, G. Raju & B.C. Kim, Buckling analysis and optimization of variable angle tow composite plates. *Thin Walled Structures,* **60**, 2012, pp. 163-172.

[6] A. Sabido, L. Bahamonde, R. Harik & M.J.L. van Tooren. Maturity assessment of the laminate variable stiffness design process. *Composite Structures,* **160**, 2017, pp. 804-812.

[7] T.J. Dodwell, R. Butler & A.T Rhead, Optimum Fiber Steering of Composite Plates for Buckling and Manufacturability. *AIAA Journal*, **54**, 2016, No.3, pp. 1139-1142.

[8] B.C. Kim, K. Potter & P. Weaver, Continuous Tow Shearing for Manufacturing Variable Angle Tow Composites. *Composites Part A: Applied Science and Manufacturing,* **43**, 2012, No. 8, pp. 1347-1356.

[9] S.W. Tsai & J.D.D. Melo, Composite Materials Design and Testing: Unlocking mystery with invariants. Stanford, CA: Composites Design Group, Department of Aeronautics & Astronautics, Stanford University, 2015. pp. 385-420.

[10] A.J. Vizzini, Strength of Laminated Composites with Internal Discontinuities Parallel to the Applied Load. *AIAA Journal,* **30**, 1992, No. 6, pp. 1515-1520.

[11] F.W. Williams, D. Kennedy, R. Butler & M.S. Anderson, VICONOPT: Program for Exact Vibration and Buckling Analysis of Prismatic Plate Assemblies. *AIAA Journal,* **1**, 1991, No. 4, pp. 497-518.

[12] D.J. Dawe & T.J. Craig, Buckling and vibration of shear deformable prismatic plate structures by a complex finite strip method. *International Journal of Mechanical Sciences,* **30**, 1988, No. 2, pp. 77-99.
[13] W.H. Wittrick & F.W. Williams. Buckling and Vibration of Anisotropic or Isotropic Plate Assemblies under Combined Loadings. *International Journal of Mechanical Sciences,* **16**, 1974, pp. 209-239.
[14] W.H. Wittrick & F.W. Williams, An Algorithm for Computing Critical Buckling Loads of Elastic Structures. *Journal of Structural Mechanics,* **1**, 1973, No. 4, pp. 497-518.
[15] ABAQUS, *ABAQUS™ Theory Manual*, Version 6.17. Dassault Systemes Simulia Corp, 2017.
[16] E.J. Barbero, *Finite Element Analysis of Composite Materials Using Abaqus™*, Chapter 4: Buckling. CRC Press, 2013.
[17] E. Riks, An incremental approach to the solution of snapping and buckling problems. *International Journal of Solids and Structures,* **15**, 1979, No. 7, pp. 529-551.
[18] A. Jumahat, C. Soutis, F.R. Jones & A. Hodzic, Fracture mechanisms and failure analysis of carbon fibre toughened epoxy composites subjected to compressive loading. *Composite Structures,* **92**, 2009, No. 2, pp. 295-305.
[19] A. Atas & C. Soutis, Strength prediction of bolted joints in CFRP composite laminates using cohesive zone elements. *Composites: Part B,* **58**, 2014, pp. 25-34.
[20] R.S. Choudhry, S.F. Hassan, S. Li & R. Day, Damage in single lap joints of woven fabric reinforced polymeric composites subjected to transverse impact loading, *International Journal of Impact Engineering,* **80**, 2015, pp. 76-93.
[21] M. L Benzeggagh, M. Kenane, Measurement of mixed-mode delamination fracture toughness of unidirectional glass/epoxy composites with mixed-mode bending apparatus. *Composites Science and Technology*. **56**, 1996, pp.439–449. (doi:10.1016/0266-3538(96)00005-X)
[22] J. Dizy, R. Palacios, S. T. Pinho, Homogenisation of slender periodic composite structures. Int. J. Sols. Struct. 50, 2013, No.9, pp.1473-1481.
[23] ABAQUS, *ABAQUS™ Theory Manual*, Section 32.5.3, Modelling with cohesive elements, Version 6.17. Dassault Systemes Simulia Corp, 2017.
[24] ASTM International. Standard test for compressive residual strength properties of damaged polymer matrix composite plates. ASTM D7137/D7137M-07.
[25] HBM, 'catman Data Acquisition Software' (2017). https://www.hbm.com/en/2290/catman-data-acquisition-software/ [Accessed 02/06/2017]
[26] Correlated Solutions, 'VIC-3D System.' http://www.correlatedsolutions.com/vic-3d [Accessed 18/05/17].
[27] G. Czel, S. Pimenta, M.R. Wisnom, P. Robinson, Demonstration of pseudo-ductility in unidirectional discontinuous carbon fibre/ epoxy prepreg composites. *Composites Science and Technology.* **106**, 2015, pp. 110-119.